SunSolve

Radiative heat loss from PV systems

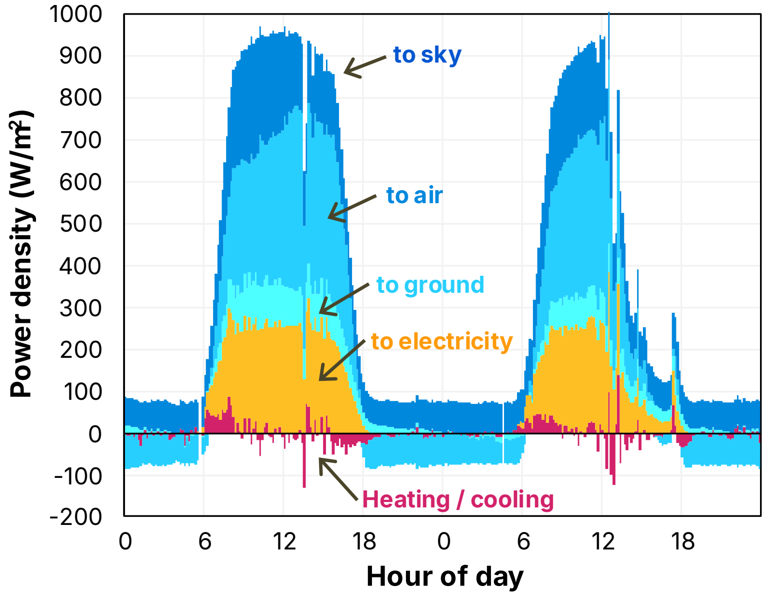

Contents

1. Summary

We investigate the radiative heat loss from the modules of a PV power plant.

Expanding on recent studies by Sandia, DTU, UNSW, 5B, FTC Solar and ourselves [1–5], we describe how radiation to the sky comprises a large fraction of the heat loss from a module, how it depends on atmospheric conditions, how it affects energy yield, and how it can be accurately forecasted.

We show that the modules of a modern PV system radiate about 30–60% of their heat to the sky during the day. This heat loss depends strongly on the sky temperature T_s, which itself depends on the ambient air temperature near the system T_a and atmospheric conditions like humidity and cloud cover. We explore these dependencies and examine T_s at six sites.

The PV industry's standard way to account for radiative heat loss is relatively simple. It assumes that radiative loss is proportional to ($T_m - T_a$), where T_m is the module temperature. In reality, however, it is more accurate to say that radiation to the sky is proportional to $v_s(\beta) \times (T_m^4 - T_s^4)$, where v_s is a view-factor that depends on the module tilt β.

Fortunately, this more realistic equation is readily incorporated into yield forecasts. It merely requires a value for β and T_s, where the latter can be taken from satellite data or estimated from the data contained in weather files. Consistent with other studies [1–5], we demonstrate that this approach can improve the prediction of T_m using data from several experimental facilities.

We then investigate the error that the standard approximation introduces into yield forecasts. We find that this error causes the predicted energy yield from a system to be more overestimated — or less underestimated — at times of high humidity and cloud cover, and vice versa. This contributes to errors in the annual yield of about ±0.5%. Perhaps more importantly, the error varies from site to site, from day to day, and from hour to hour, because it depends on atmospheric conditions that can be erratic or have seasonal trends. At a typical site, the error in daily yield varies by ~0.8% for single-axis trackers and ~1% for fixed east–west systems. This error can be mitigated by applying the more realistic approach to radiative heat loss, now available in the SunSolve Yield software.

We hope this white paper inspires additional thermal experiments and, ultimately, assists the PV industry to make more accurate yield forecasts.

2. Heat loss from PV modules

PV modules produce less power when they are hotter. Roughly speaking, if a module is 3 °C hotter, it produces 1% less power. And since modules typically operate at temperatures between T_m = 10 °C and 60 °C, we cannot accurately predict their output power unless we can accurately predict their temperature.

The most common way to predict T_m is with the simple formula,

$$\Phi \cdot (\alpha - \eta) = U \cdot (T_m - T_a), \qquad (1)$$

where T_a is the temperature of the ambient air, Φ is the irradiance incident to the module, α is the absorptance, η is the module efficiency, and U is the 'U-value', the module's thermal transmittance, which describes how readily the heat flows into and out of the module. Thus, a higher U-value leads to a lower T_m.[1]

Eq (1) is a simple way to account for all three modes of heat transfer:

1. Conduction, where heat flows from the modules through the structural supports and into the ground.
2. Convection, where heat flows from the surface of the module into the air. This heat loss increases as wind speed increases.
3. Radiation, where heat is emitted by long-wavelength photons into the sky and into other objects like the ground or neighbouring buildings.

Thus, when U is assumed constant, which is common in PV forecasts, the right-hand-side of Eq (1) treats all three mechanisms as being proportional to $T_m - T_a$. In reality, however, this is an approximation. But does that matter?

This white paper explores the third mode of heat transfer, the radiative heat loss. It describes how radiative loss to the sky is a significant fraction of the total heat loss, how it depends on atmospheric conditions, and how one can account for it without introducing any new variables. The white paper also quantifies the error entailed in the simple approximation of Eq (1).

We conclude that accounting for radiative loss with a more realistic approach is relatively easy and more accurate.

[1] Eq (1) states that the solar energy absorbed by the module that does not produce electricity (the left-hand side) equals the heat lost from the module (the right-hand side). The parameter Φ is often called the plane-of-array (POA) irradiance. The absorptance α is almost always assumed to be 0.9; thus, uncertainty in α is effectively absorbed into U.

3. Radiation to the sky

Equations

The right-hand side of Eq (1) is the total heat flowing out of the module Q_{tot}. We can re-express it as being the heat lost to the ambient Q_a and to the sky Q_s:

$$Q_{\text{tot}} = Q_a + Q_s. \tag{2}$$

The thermal model in standard PV forecasts effectively treats Q_s as

$$Q_s = U_s \cdot (T_m - T_a), \tag{3}$$

where U_s is the radiative component of the total U-value,[2] but a more accurate description is

$$Q_s = \sigma \cdot \epsilon \cdot \nu_s \cdot (T_m^4 - T_s^4), \tag{4}$$

where σ is the Stefan–Boltzmann constant, ε is the emissivity of the module, ν_s is the view-factor (the effective fraction of the sky 'seen' by the module), and T_s is the temperature of the sky [1].

Eq (4) has three important features. Firstly, Q_s decreases as the view factor decreases and, hence, as the panel's tilt increases.[3] Thus, radiative losses are greatest when the module is horizontal. Secondly, Q_s depends on T_s, which itself depends on atmospheric conditions. As we'll see, on clear dry days, the sky can be as cold as –40 °C, whereas on humid overcast days, it can be close to T_a. This means that radiative loss depends on the weather and must vary from day to day and site to site. Thirdly, Q_s is non-linear, having a T^4 dependence, although, perhaps surprisingly, this has little impact over the T range of interest.

These features mean that when radiative loss is significant — and it usually is — Eq (3) is only a rough approximation of the radiative heat loss.

Error due to the standard approximation

We next assess the error arising from treating Q_s with Eq (3) rather than Eq (4). This error will, of course, depend on the weather conditions, and the example we give approximates a sunny day with a light breeze.

[2] This is equivalent to treating the total U-value as the sum of two components, $U = U_a + U_s$, where U_a and U_s govern the heat flow into the ambient air and the sky.

[3] For a module far from the edge of a system, the view factor depends on the module pitch P, their length L, and the tilt β by $\nu_s = \left[(1 + P/L) - \sqrt{(P/L)^2 - 2(P/L)\cos\beta + 1}\right]/2$ [6].

We set our example system to have a total U-value of U_{tot} = 29 W·m^{2}·K^{-1}, which is the standard value used in PV yield forecasting of free-standing systems, and we set the other parameters to represent a typical operating point: T_m = 50 °C, T_a = 20 °C, T_s = −10 °C and β = 30°.[4] Under these conditions, the radiative loss is calculated with Eq (4) to be 279 W/m^2, and by applying Eq (3), we find that this heat loss equates to an effective U_s of 9.3 W·m^{2}·K^{-1}.

Thus, with the example inputs, 32% of the total heat loss is radiated to the sky.

What happens if there is a change in module temperature? Or sky temperature? Or module tilt?

The standard approach, which applies Eq (3), assumes that U_s remains constant. In reality, however, such changes do affect the radiation to the sky, and U_s does not remain constant at 9.3 W·m^{2}·K^{-1} for all conditions. Instead, U_s decreases as T_m, T_a and β increase, as quantified in the appendix (see Figure 22).

Thus, the standard approach introduces an error into its calculation of T_m. How big is that error in T_m?

Figure 1 answers this question for our example system. It plots the error in T_m if the radiative contribution were computed with Eq (3) and U_s = 9.3 W·m^{2}·K^{-1} for all conditions instead of Eq (4). The figure shows that the error in T_m varies by about ±4 °C when just one parameter is varied over a large range.[5]

We'll explore later how this error affects yield forecasts, but before then, we investigate the sky temperature.

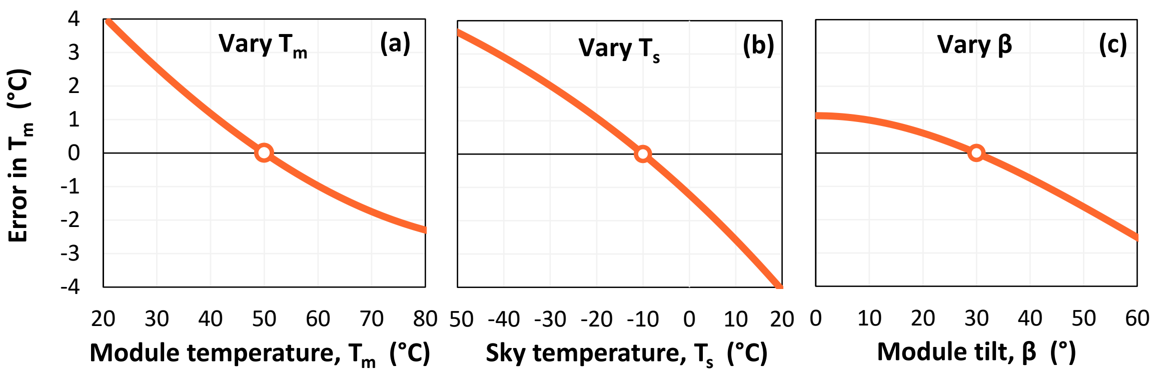

Figure 1: Error in predicted module temperature when using Eq (3) instead of Eq (4) plotted for a range of **(a)** T_m, **(b)** T_s and **(c)** β for the example conditions.

[4] We have also assumed ε = 0.9, and computed v_s from β = 30° assuming P = 5 m, L = 2 m, and an isotropic sky approximation (see Footnote 3).

[5] The error is defined as $T_m' - T_m$, where T_m' is the incorrect T_m when using Eq (3) instead of Eq (4). It is calculated from $Q_{tot} = 29 \cdot (T_m' - T_a)$, where $Q_{tot} = U_a \cdot (T_m - T_a) + Q_s$, U_a is the non-radiative U-value equal to 19.7 W·m^{2}·K^{-1} (i.e., 29 – 9.3), and Q_s is determined with Eq (4).

4. Sky temperature

Worldwide

Sky temperature T_s can be evaluated by satellite measurements of downwelling longwave radiation ('downwelling'),[6] where higher downwelling equates to a higher T_s. Figure 2 plots downwelling throughout the world, showing that T_s tends to be much higher — and less variable — near the equator. T_s also tends to be lower in colder or drier climates.

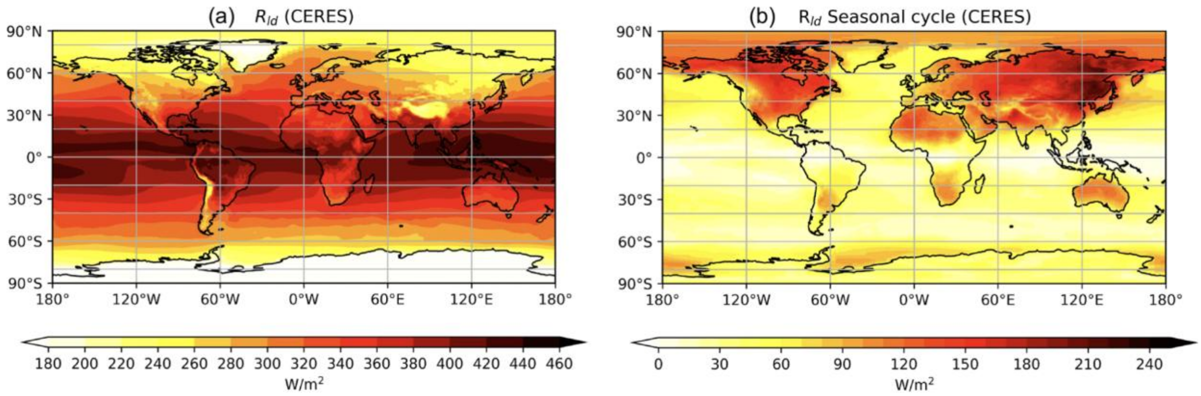

Figure 2: Global downwelling longwave radiation, where **(a)** plots the annual average and **(b)** plots the seasonal variation. Image from [7].

Two example locations

To learn more about sky temperature, we extracted T_s from ERA5-land satellite data [8] for two very different sites:

(a) Albuquerque, USA — a clear inland climate; and

(b) Roskilde, Denmark — a cloudy coastal climate.

Figure 3 plots T_s against the ambient temperature T_a at the two sites. It demonstrates how (i) T_s and T_a follow the same seasonal trends, (ii) T_s is always lower than T_a, and (iii) the difference between T_s and T_a is much greater in the clear climate than it is in the cloudy climate.

The most important difference between the climates for this study can be construed from Figure 4, which plots T_s vs T_a for each site. It shows that for the same air temperature, the sky is 10–20 °C cooler in Albuquerque than in Roskilde.

[6] Downwelling longwave radiation is a measurement of the infrared radiation emitted by the atmosphere in the direction of the Earth's surface, it is proportional to $\sigma \cdot T_s^4$, as described further in appendix C.

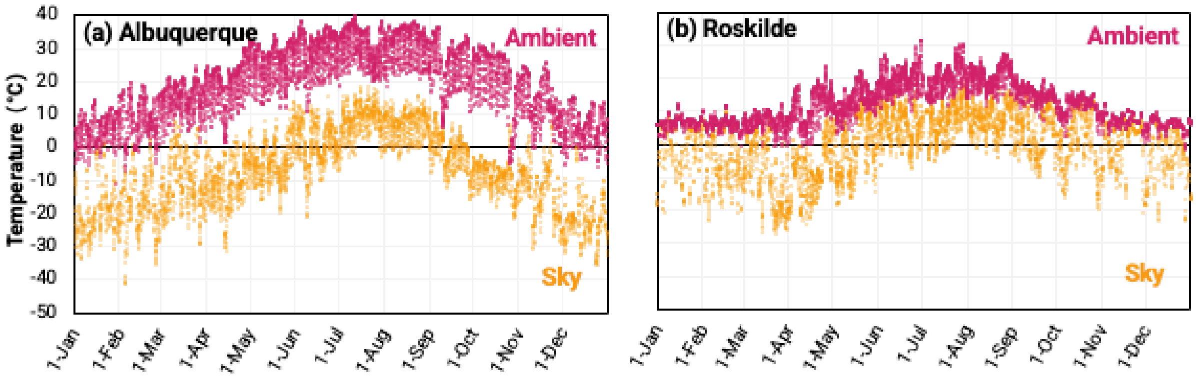

Figure 3: Sky temperature calculated from ERA5 satellite data and ambient temperature measured in 2020 at Albuquerque (Sandia National Laboratories) and Roskilde (Denmark Technical University).

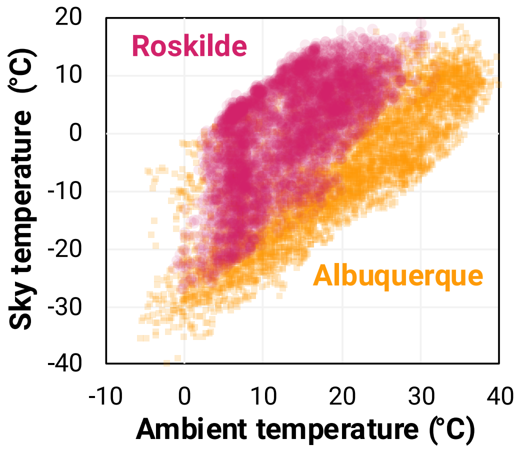

Figure 4: Sky vs ambient temperature measured at Albuquerque and Roskilde in 2020.

Thus, with all other conditions being equal, we expect that modules installed in Albuquerque should emit more radiative heat — and hence be cooler and more efficient — than modules installed in Roskilde. This is indeed the case, as we'll quantify in Section 6 for two system configurations.

What affects sky temperature?

In addition to T_a, the main atmospheric conditions that influence T_s are humidity and cloud cover. As humidity and cloud clover increase, T_s also increases, which largely explains the difference between clear dry Albuquerque and cloudy humid Roskilde. We explore that further in the appendix on sky temperature models. Other atmospheric effects that influence T_s are greenhouse gases (e.g., CO_2, CH_4), large aerosol particles cloud-base height, sky emissivity, and atmospheric pressure [7].

T_s variability

Since sky temperature depends on T_a and atmospheric conditions, it not only varies between sites, but also varies from day to day and from hour to hour.

Figure 5 plots four consecutive days for T_s, T_a, humidity, and the diffuse fraction at Albuqerque. It demonstrates how on the third day, which was cloudy and humid, the sky temperature was 10–15 °C higher than on neighbouring days, which were clearer and drier. The figure also shows how T_s changes by up to 15 °C on clear days but is more stable on the cloudy day.

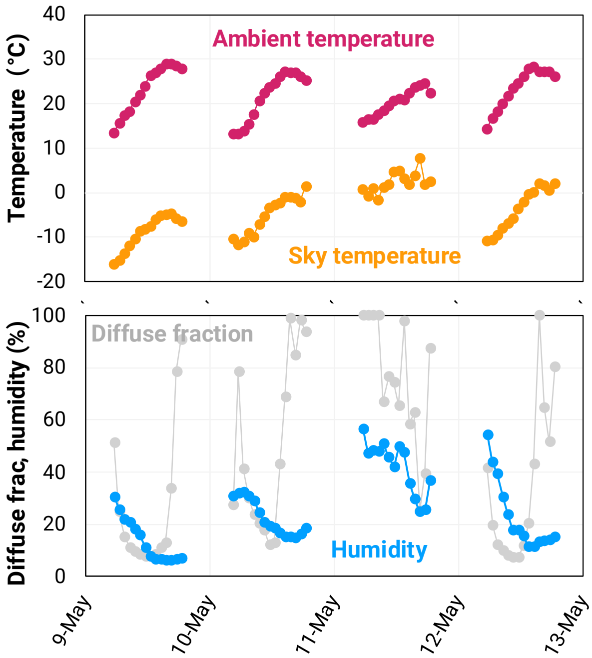

Figure 5: Sky vs ambient temperatures measured at Albuquerque over four days in 2020. The diffuse fraction and humidity are also plotted.

Summary

The radiative loss from a PV module depends on the sky temperature T_s, which itself depends strongly on the air temperature near the system, as well as on humidity, cloud cover, aerosols and greenhouse gases. We can extract T_s from satellite data or, less accurately, we can predict it from typical weather data and models such as those in the appendix. But is it worth the effort? We next assess experimental data to see whether a more realistic accounting of radiative losses — one that uses T_s — can help predict module temperature more accurately.

5. Experimental evaluation

We now investigate whether the measured module temperature can be predicted more accurately by using the realistic equation for radiation, Eq (4), rather than the simple equation, Eq (3).

The analysis is performed on data from five test facilities over four locations, as listed in Table I. They include three types of system configurations: single-axis trackers (SATs), fixed-tilt systems and Mavericks.[7]

Table I: Sites examined in this study and the duration of the data in months.

Test facility	Location	System configuration	Module	Refs	Months
FTC Solar	Denver, USA	Single-axis tracker	Bifi PERC	[2]	1.5
Sandia	Albuquerque, USA	Fixed-tilt, 35°	Mono-PERC	[3]	12
Sandia	Albuquerque, USA	Fixed-tilt, 35°	Mono-HIT	[3]	12
5B	Bungendore, Aus	Maverick, 10°	Mono-PERC	[4,5]	3
DTU[8]	Roskilde, Denmark	Single-axis tracker	Mono-PERC	[3,9]	12

Example days

Figure 6 plots the measured T_m and T_a for the SAT at Denver over two days in August. The first day is warm with clear skies and the second day is cooler with increasing cloud.

The figure also plots the predicted T_m for three models: M1, M2 and M3. Each model predicts T_m from measurements of T_a, T_s and Φ, which we'll describe

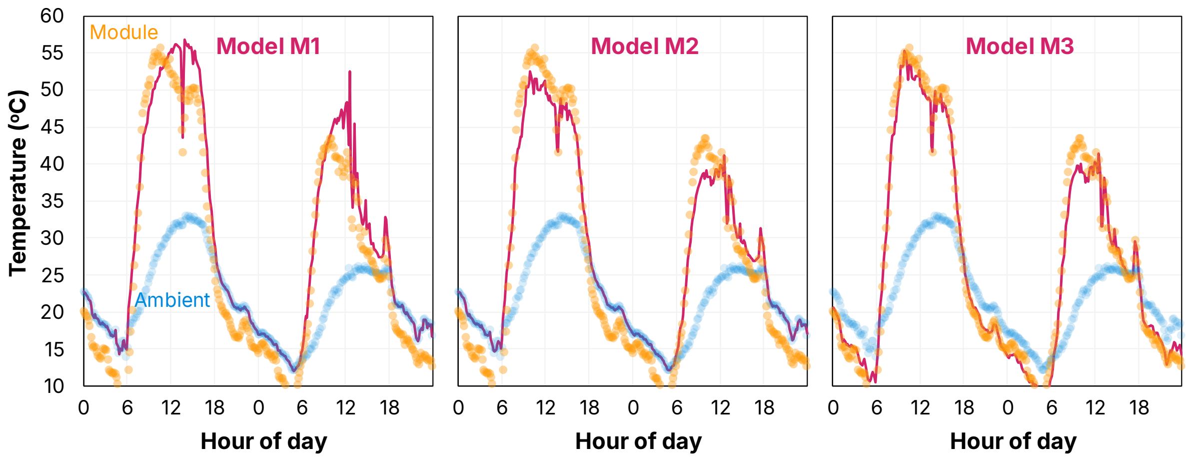

Figure 6: Measured T_m (orange), measured T_a (blue) and modelled T_m (pink) for models M1, M2 and M3 for the FTC SAT on 27 and 28 August 2021.

[7] A Maverick system contains modules facing both east and west and tilted at 10° (refer to www.5b.co). It is referred to as a 'wave' or a 'dome' in SunSolve and PVsyst, respectively.

[8] Using data from [3] except for a different T_{amb} sensor, now believed to be more accurate.

below, but in brief, M1 is the standard model, M2 is a refined model that still retains the simplistic radiative equation, and M3 is identical to M2 but with the realistic radiative equation.

The figure illustrates how the discrepancy between the predicted and measured T_m decreases as the model becomes more complex. Of most relevance to this white paper, a comparison of M3 to M2 indicates that the discrepancy decreases markedly after the realistic approach to radiative losses is introduced.

Comparison of thermal models

Figure 7 presents the results of the three models when fitted to all data from each site. Following the procedure described in the appendix, it assesses the thermal models by their RMSE for daytime data, a statistical metric that quantifies the discrepancy between the predicted and measured T_m. (RMSE effectively combines the mean bias error, MBE, and the scatter about that bias.)

The results for RMSE can be contextualised by remembering that a 95% confidence interval equates to 2 × RMSE. Thus, for the SAT at Denver, Model 1 gives us 95% confidence that we can predict T_m to within ±9 °C at any point in time. By contrast, Model 3 predicts T_m to within ±3.6 °C.

For the purpose of this study, the general form of the thermal models is

$$\Phi \cdot (\alpha - \eta) = k \frac{dT_m}{dt} + Q_{tot}, \quad (5)$$

which states that the irradiance absorbed by the module but not extracted as electricity (LHS) either changes the temperature of the module over time dT_m/dt or emanates as heat from the module Q_{tot}. Thus, it incorporates transient effects.

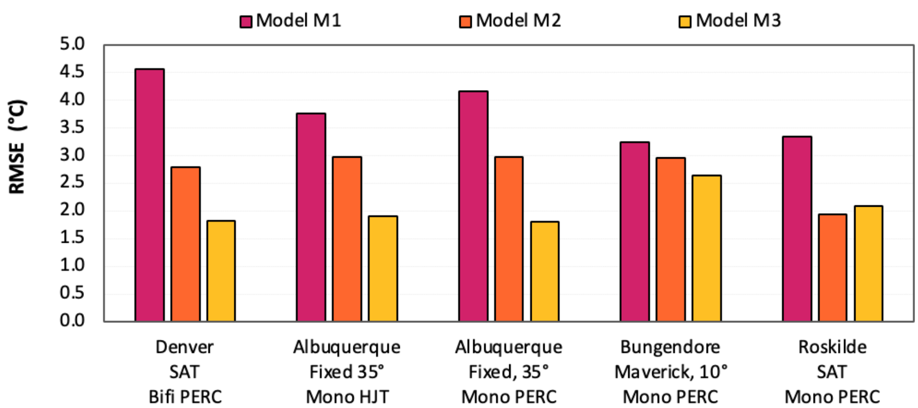

Figure 7: RMSE for the five systems and three models.

Model M1 — standard approach

M1 represents the approach applied in most PV yield forecasts when no operational data is available for calibration. It assumes that transient effects are negligible, $dT_m/dt = 0$, and that Q_{tot} is given by Eq (1) with $U = 29\ W{\cdot}m^{-2}{\cdot}K^{-1}$,

$$Q_{tot} = 29 \cdot (T_m - T_a). \qquad (6)$$

We can consider this the simplest model used in forecasting, and it effectively lumps all heat transfer modes together, thereby incorporating radiative loss to the sky into its U-value and assuming it is proportional to ($T_m - T_a$). The value of 29 $W{\cdot}m^{-2}{\cdot}K^{-1}$ was derived from a few experiments in the 1990s and has remained widespread ever since [10].

Figure 7 shows that M1 has an RMSE of 3.2–4.5 °C for the five sites.

Model M2 — calibrated Faiman with transients

M2 attains close to the lowest RMSE without introducing the realistic equation for radiative loss to the sky. M2 extends Q_{tot} to include the wind speed w,

$$Q_{tot} = (U_c + U_v \cdot w) \cdot (T_m - T_a), \qquad (7)$$

it uses best-fit values of U_c and U_v to the experimental data, and it accounts for transient effects.[9] It can be considered a calibrated Faiman equation extended to include transients, and it accounts for the main effects that introduce discrepancy between the model and measurements of T_m, other than radiation to the sky. It has two free variables, U_c and U_v.

Importantly, M2 continues to treat radiative loss with the simple approach, Eq (3), thereby assuming it remains proportional to ($T_m - T_a$) and incorporating it into U_c. If we wanted to distinguish between the heat lost to the ambient and the sky, we would rewrite the equation as

$$Q_{tot} = \left(U_{c\_a} + U_v \cdot w\right) \cdot (T_m - T_a) \quad + \quad U_s \cdot (T_m - T_a), \qquad (8)$$

where U_{c_a} accounts for heat loss to the ambient excluding forced convection, and U_s accounts for heat loss to the sky. Thus, $U_{c\_a} = U_c - U_s$. We use this equation in Section 6 once we have an estimate for U_s.

[9] Where $k = m \cdot c / A$, and where m is the mass, A is the module area, and c is the heat capacitance, which was computed from the materials and dimensions of the modules.

Figure 7 shows that M2 greatly reduces the discrepancy between the predicted and measured T_m compared to M1. It decreases by between 0.6 and 2.8 °C at the five sites. This indicates that although the standard approach gives a reasonable prediction of the measured T_m, the prediction can be greatly improved by accounting for wind and transient effects, and by calibrating the model.

Model M3 — calibrated Faiman with transients and realistic radiative loss

Finally, we extend M2 to introduce the more realistic equation for radiative loss, Eq (4), giving

$$Q_{tot} = \left(U_{c\_a} + U_v \cdot w\right) \cdot (T_m - T_a) \; + \; \sigma \cdot \epsilon \cdot v_s \cdot (T_m^4 - T_s^4). \qquad (9)$$

The first and second terms represent the heat loss to the ambient and to the sky, respectively. Thus, M3 has two free variables, U_{c_a} and U_v, which is the same number as in M2.[10]

In this study, we determine T_s from ERA5 downwelling data. This is similar to Driesse *et al*. [1], Hamer *et al*. [4], and Kim *et al*. [5] but rather than using downwelling directly, we convert it to an effective T_s to remain consistent with the focus of this white paper (i.e., the dependence of radiative loss on T_s). As explained in Appendix C, this does not introduce any additional error.

A comparison of RMSE between M2 and M3 therefore tells us whether accounting for changes in Q_{tot} that arise from radiative losses being proportional to $v_s \times (T_m^4 - T_s^4)$ rather than $(T_m - T_a)$ reduces the discrepancy between model and experiment.

Figure 7 indicates that for three of the five systems, the discrepancy between the predicted and measured T_m decreases markedly, by 1.0–1.2 °C, when the realistic approach to radiative loss is introduced (compare M3 to M2). We see a smaller improvement in RMSE at Bungendore (0.3 °C) and a slight deterioration at Roskilde (for which T_s tends to be much closer to T_a than the other sites).

We conclude that the thermal behaviour of an experimental PV system can, in some cases, be more accurately predicted by a model that includes a realistic

[10] Here, and in all other calculations in this white paper, we assume $\varepsilon = \alpha = 0.9$. Any error in these values is effectively absorbed into the calibrated (best-fit) U-values. E.g., if the actual ε is 2% higher than 0.9, U_s will be underestimated by 2% and hence the best fit U_a will be an overestimate of the true value. We also calculate v_s from the isotropic sky approximation.

accounting of radiative loss to the sky. We emphasise, however, that the improvement from applying the realistic radiative equation and T_s is greatest when larger sources of discrepancy, like wind speed and transient effects, are removed (see Appendix B); and that to some extent, the investigation of RMSE is limited by experimental noise and systematic error in measurements of T_m, T_a, T_s and Φ.

Heat loss breakdown vs time

Once an accurate thermal model has been established, it can be used to evaluate an operational power plant. We give an example for the SAT at Denver using a model that has been even further refined than M3 such that it includes conductance to the ground and the influence of tilt and wind direction on convection (see [2] and Appendix B).

Figure 8 plots what happens to the incident solar energy for the two example days at Denver. It shows how a large fraction of the power emanating from a PV module during the day is radiated to the sky. The figure also reveals a curious effect at nighttime whereby heat flows from the ambient air into the module and radiates from the module to the sky [1–5, 14]. As described in the appendix, this provides a useful way to investigate heat-loss mechanisms, but only when the

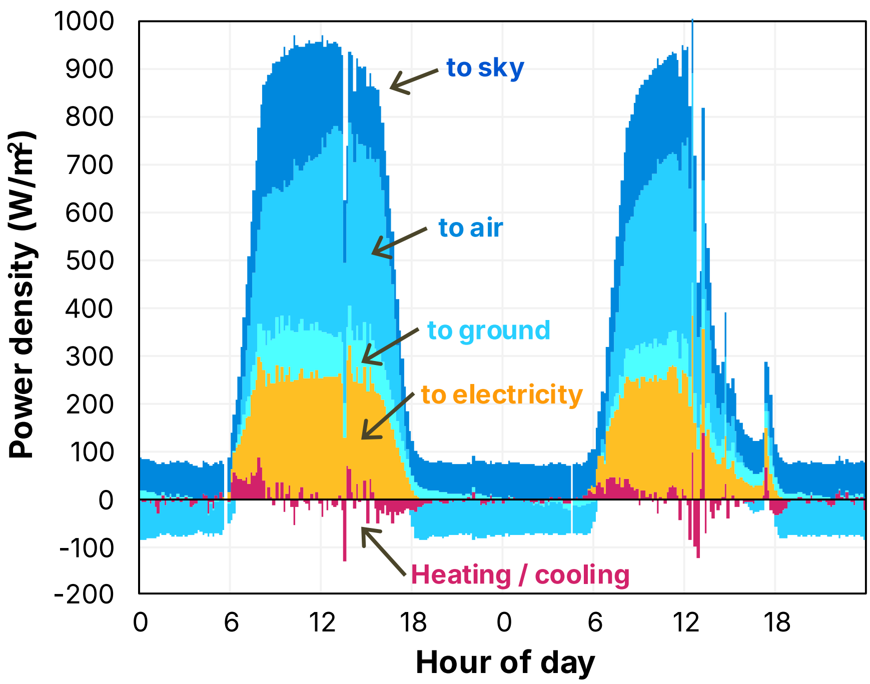

Figure 8: Modelled energy outflow for the FTC SAT at Denver on 27 and 28 of August 2021.

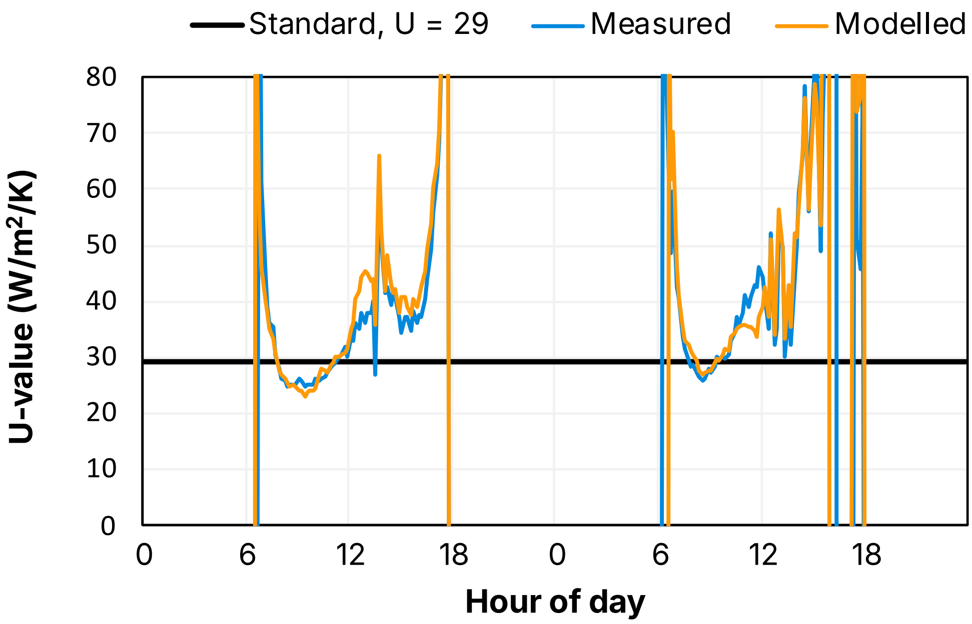

Figure 9: Measured and modelled U-value calculated with Eq (1) compared to the standard value of 29 W·m^{2}·K^{-1}. Data ploted for FTC SAT near Denver on 27th and 28th of August, 2021.

realistic model of radiative heat transfer is used. Note further, that accounting for transient effects allows one to plot the energy consumed or emitted when the temperature of the module changes.

Figure 9 plots the U-value when defined by Eq (1) for the same two days. We see how the U-value tends to increase when it is cloudy and on the shoulders of the day, both of which relate to radiative loss to the sky. Furthermore, the figure shows how, on these particular days, the measured U-value is far from the oft-assumed value of 29 W·m^{2}·K^{-1}. In addition to changes in radiative heat loss, the measured U-value depends strongly on wind speed.

Summary

We have seen that module temperature T_m can be more accurately predicted by using the realistic radiative equation. This indicates that radiative heat loss is both significant and more dependent on T_s than T_a.

6. Radiative heat loss in yield forecasts

We end this study by examining how radiative heat loss affects yield forecasts. In particular, we quantify how radiative heat loss varies from site to site, and we calculate the error introduced by using the simple approach to radiative loss; that is, by treating it as being proportional to ($T_m - T_a$) instead of $v_s(\beta)\times(T_m^4 - T_s^4)$.

Sites

We investigate six sites. These include the same four sites examined in Section 5, plus another two that have more extreme climates: Singapore and Chajnantor. Singapore is cloudy, humid, and near the equator; its T_s is relatively warm and stable, being between 15 and 25 °C all year round. Chajnantor is in the Atacama desert where the weather is cold, dry and clear; its T_s is cool and variable, being between –50 and 0 °C.

Figure 10 plots T_s against T_a for all six sites. It shows how the sites represent a variety of climates within the {T_a, T_s} parameter space, and how they can be compared using the Swinbank line defined in the caption. We see that data for humid locations, like Singapore and Roskilde, lie well above the Swinbank line, whereas data for drier locations, like Chajnantor and Albuquerque, lie below. Interestingly, the sites also exhibit different slopes in the data (i.e., trends).

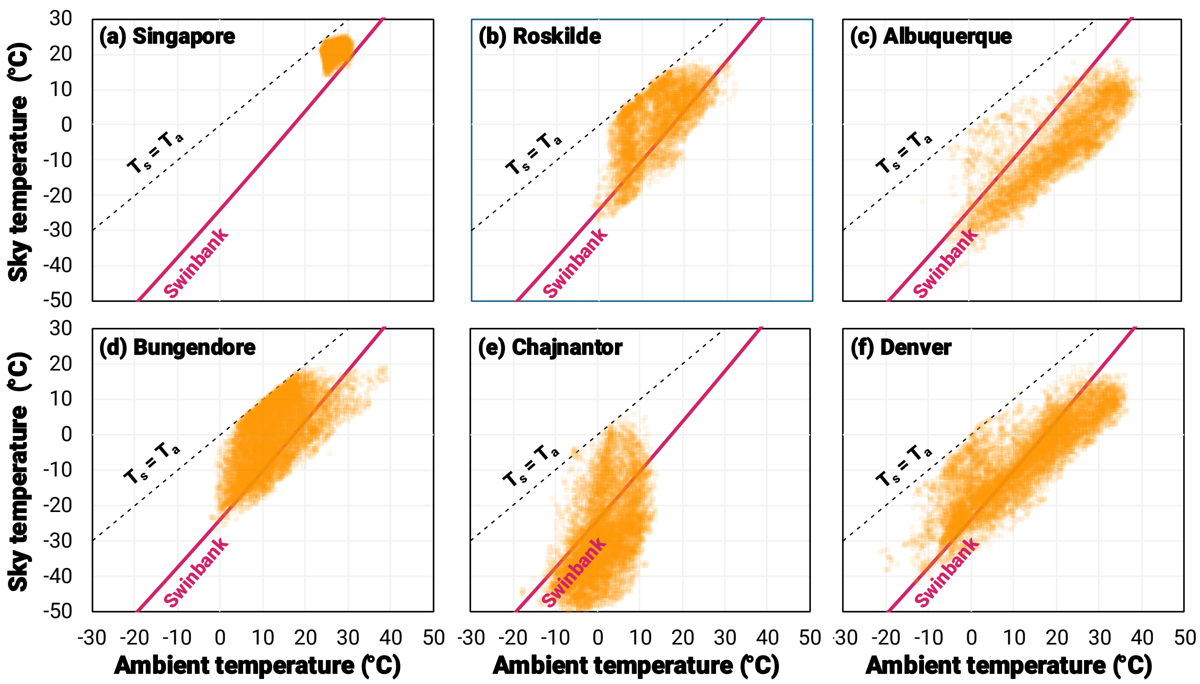

Figure 10: T_s vs T_a for **(a)** Singapore, **(b)** Roskilde, **(c)** Albuquerque, **(d)** Bungendore, **(e)** Chajnantor and **(f)** Denver. The Swinbank line follows T_s = 0.0552×$T_a^{1.5}$ [11].

Approach

Since our focus is radiative heat loss to the sky Q_s and, in particular, the error arising from the standard approximation that Q_s is proportional to $(T_m - T_a)$, we treat the remaining sources of heat loss as being identical for all sites; that is, we assume they all follow $Q_a = (U_{c\_a} + U_v \cdot w) \times (T_m - T_a)$.

We then define the error to be the difference in yield that arises when determining Q_s with using Eq (3) instead of Eq (4). This is equivalent to the relative difference between Models M2 and M3 in Section 5.

The analysis is applied to SATs and Mavericks using weather from 2020. We set the U-values to be those that gave the best fit to the experiments at Bungendore and Denver, as listed in Table II. Although those values might contain experimental error, they are applied equally at all sites in these calculations, so the most important outcome of this study is the calculation of how the error varies between sites, rather than the absolute error itself.[11]

Table II: U-values applied in these calculations.

Parameter	Represents	SAT	Maverick
U_v	Forced convection	3.2	3.2
U_{c_a}	Heat loss other than forced convection and radiation to the sky	15.5	11.2
U_s	Radiation to the sky (simplistic approach M2)	8.3	11.9

Results — error in the annual yield

Table III presents the annualised results. It shows that about half of the total annual heat loss during the day is emitted by radiation to the sky. For SATs, the fraction is 30–50% and for Mavericks it is 35–60%. The radiative fraction is greater for Mavericks because of their low tilt angle.[12]

Table III lists the sites in order of this radiative fraction, where the fraction tends to be lower at more humid sites (where T_s is higher), at windier sites (where convection is higher), and at sites with higher irradiance (and hence higher T_m).

Table III also shows that the error in the average T_m varies from –0.5 to +2.3 °C, and that the error in the annual yield varies from –0.5% to +0.4%.

[11] Interestingly, those calibration studies find U_v to be significantly higher than is often assumed.

[12] We saw earlier that a lower β increases $v_s(\beta)$. Moreoever, Φ is also lower, which tends to a lower T_m, which reduces the Q_a contribution more than the Q_s contribution.

Table III: Comparison of the error introduced into the average daytime T_m and annual yield when using the standard approximation for radiative heat loss.

	Singapore	**Roskilde**	**Albuquerque**	**Bungendore**	**Chajnantor**	**Denver**
Köppen–Geiger class	Tropical rainforest	Oceanic	Cold semi-arid	Oceanic	Cold desert	Cold semi-arid
Average daytime weather						
T_a (°C)	27.5	13.1	19.8	14.9	3.5	15.3
T_s (°C)	21.5	0.3	−6.6	1.2	−27.3	−5.7
WS (m/s)	4.3	2.2	2.3	4.6	5.1	4.0
RH (%)	74.8	73.3	28.1	–	35.6	40.5
Yield (kWh/m²)						
SAT	363	263	513	387	694	485
Maverick	349	221	410	352	592	420
Radiative fraction						
SAT	31%	38%	39%	43%	45%	49%
Maverick	36%	51%	53%	52%	57%	61%
Average daytime T_m (°C)						
SAT	34.4	18.3	30.1	21.7	15.0	23.4
Maverick	34.8	17.4	27.6	21.3	13.6	22.3
Best fit U_s ($W \cdot m^{-2} \cdot K^{-1}$)						
SAT	7.8	9.0	11.1	9.7	9.7	10.4
Maverick	8.8	11.7	14.0	11.6	11.9	13.3
Average error in T_m (°C)						
SAT	+0.1	+0.9	+2.0	+1.4	+1.1	+1.4
Maverick	−0.4	+0.9	+2.3	+0.5	+0.8	+1.3
Error in annual yield						
SAT	+0.1%	−0.1%	−0.5%	−0.2%	−0.2%	−0.3%
Maverick	+0.4%	+0.0%	−0.4%	+0.0%	+0.0%	−0.2%

We stress that this error is small because (i) U_s for Model M2 has been calibrated such that the error will be near zero at the calibration site, and (ii) the error is just the error arising from applying the simplistic approach to radiative heat loss (Eq (3) instead of Eq (4)). Hence, the absolute error is not so relevant. Instead, the best way to interpret these results is by the variation between sites.

In relation to the site-to-site variation in the predicted error, we find that

- the average T_m varies by 1.9 °C for SATs and 2.7 °C for Mavericks,
- the annual yield varies by 0.6% for SATs and 0.8% for Mavericks.

This is equivalent to the site-to-site variation in the best fit U_s being 3.3 $W \cdot m^{-2} \cdot K^{-1}$ for SATs and 5.2 $W \cdot m^{-2} \cdot K^{-1}$ for Mavericks.

Results — error in daily yield

PV engineers are often interested in a system's electrical output at a particular time of day, or a particular day of year, or for a particular weather condition like overcast or clear skies.

For instance, the capacity test for a PV power plant might be a three-week period that falls within winter or summer, or under cloudier or sunnier conditions. Or, a PV power plant might be exposed to dynamic pricing, whereby the sales price for the electricity depends on time of day and year.

It is therefore pertinent to investigate how the error depends on time and weather.

Figure 11 plots the error in the daily yield over the course of the year. It shows both seasonal trends and day-to-day scatter due to changing weather. For example, the error in a forecast at Roskilde would be 0.4% lower in winter than in summer; and the day-to-day variation in error is about 0.8%. We summarise those sources of variation for all sites in Figure 12.

We learn from Figure 11 and Figure 12 that the seasonal variation depends strongly on the site. For example, there is almost no seasonal variation in Singapore, where the humidity is similar most of the year round, but ~1% seasonal variation in Chajnantor. We also learn that the error is not necessarily more positive in summer than winter, or vice versa, because the error depends more on atmospheric conditions than it does on air temperature or irradiance.

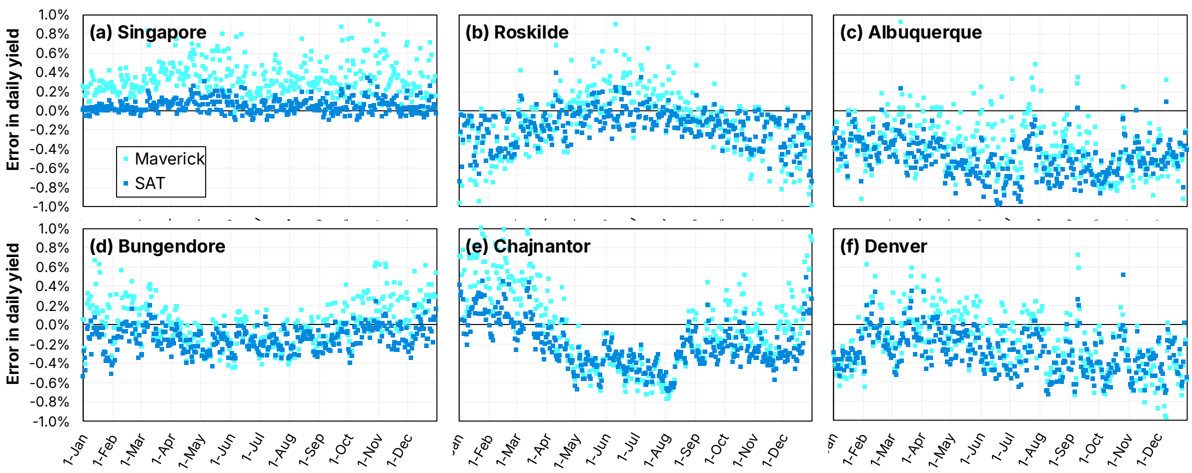

Figure 11: Relative error in the daily yield when radiative losses are treated with the simplistic rather than realistic equation, plotted against day of year.

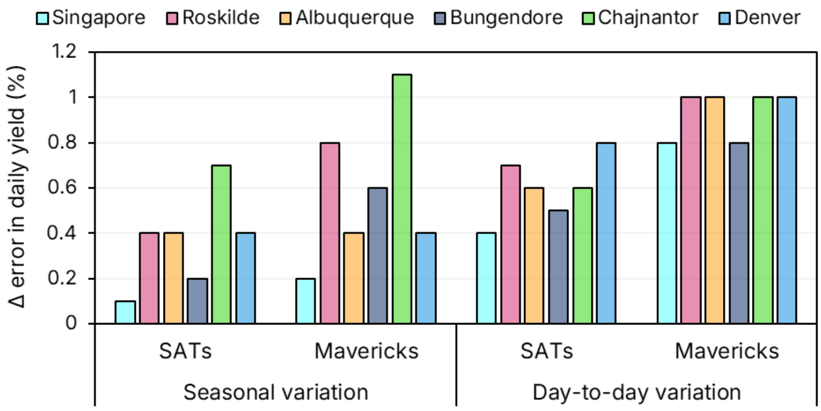

Figure 12: Variation in error of the predicted daily yield when using the simple radiative equation. Day-to-day variation is the noise on top of the seasonal variation.

Figure 11 and Figure 12 also show that day-to-day variation in error is significant for all sites, being 0.4–0.8% for SATs and 0.8–1.0% for Mavericks. This variation comes from the erratic nature of the weather.

We learn more with Figure 13, which shows how the yield is increasingly underestimated as T_s decreases below T_a. That is, when the sky is colder than usual (relative to the ambient air), the radiative loss to the sky increases, the module operates at a lower temperature, and the yield is higher than expected.

The figure shows that at a site where $T_a - T_s$ varies only a little, like Singapore, the variation in yield for SATs is no more than 0.2%; at more typical sites, the variation is ~0.8%; and in a site where it varies a lot, like Chajnantor, the variation is about 1%. Moreover, the variability in error is greater for Mavericks than for SATs because they operate at lower temperatures and have a low tilt. We expect a fixed system to be somewhere in between.

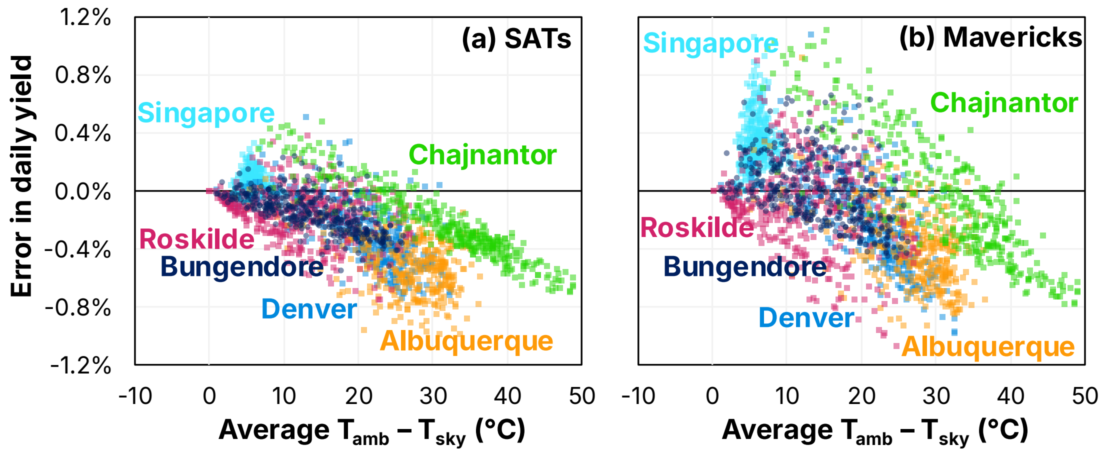

Figure 13: Relative error in the daily yield of **(a)** SATs and **(b)** Mavericks plotted against the difference between ambient and sky temperature, $T_a - T_s$.

Figure 14 shows how the error in yield correlates to (a) humidity and (b) diffuse fraction, which is roughly equivalent to cloud cover. These are the two atmospheric conditions that have the greatest impact on T_s. The figure shows how the relative error becomes more negative as humidity and cloud cover decrease.

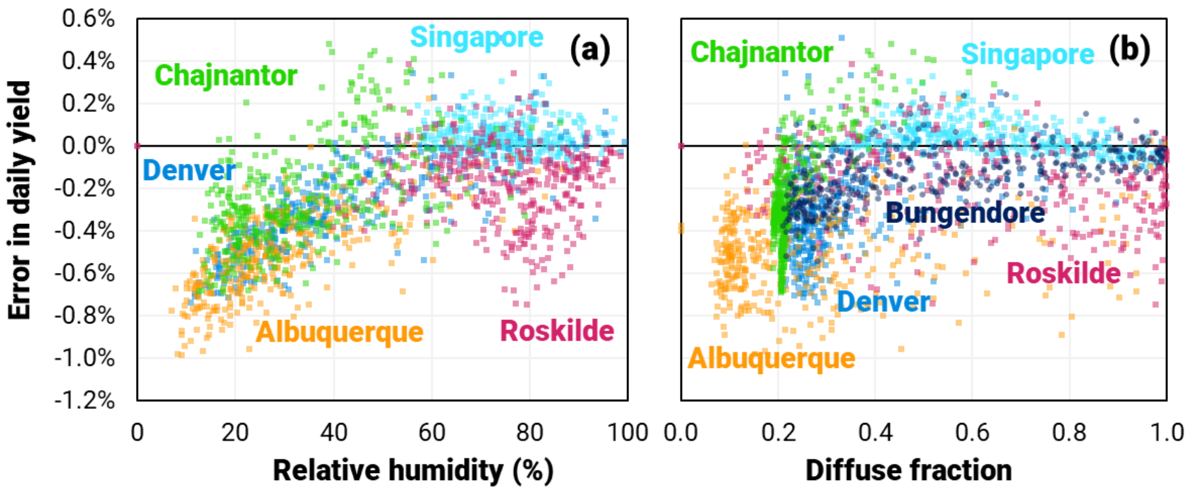

Figure 14: Relative error in the daily yield for SATs plotted against **(a)** relative humidity and **(b)** diffuse fraction. Input values calibrated to a three-week period in Denver.

Summary

We investigated the error introduced by using the simplified approach to radiative losses. We found that the energy yield from a system will be more overestimated (or less underestimated) at sites or at times of high humidity and cloud cover.

Although the absolute error depends on the choice of U_c and U_v (and, in particular, how they were calibrated), it remains instructive to observe the variation in error when one changes the site, the season, or the atmospheric conditions.

We found that,

- from site to site, the error in the annual yield varied by 0.6% for SATs and 0.8% for Mavericks;
- from winter to summer, the error in the daily yield varied by about 0.4% for most sites
- from day to day, the error in the daily yield varied by 0.4–0.8% for SATs and 0.8–1.0% for Mavericks.

7. Conclusion

During the daytime, 30–60% of the heat lost from a PV module is radiated to the sky. A conventional forecast assumes this radiative heat loss to be proportional to $(T_m - T_a)$ when, in reality, it is proportional to $v_s(\beta)\cdot(T_m^4 - T_s^4)$.

This 'standard approximation' leads to error in a forecast because, while T_s is roughly proportional to T_a, it also depends on atmospheric conditions, like humidity, cloud cover, aerosols and greenhouse gases.

Using the standard approximation for radiative heat loss instead of the more realistic equation — that is, using Eq (3) instead of Eq (4) — introduces an error in the predicted module temperature of up to ±4 °C.

We found that one can predict the measured module temperature more accurately with the realistic equation. This requires an estimate of T_s, which can be taken from satellite measurements of downwelling [1, 4, 5], or less accurately, from a parameterisation like the Swinbank and Bliss models. We demonstrated this with five systems, including SATs, fixed-tilt systems and Mavericks.

Finally, we showed that the standard approximation introduces error in the annual yield that varies from site to site by ~0.5%, and error in the daily yield that varies by ~1% throughout a year. It causes the yield to be more overestimated — or less underestimated — on humid days, and vice versa.

Since radiative losses vary from site to site, and from day to day, and since they can be more accurately modelled with Eq (4) than the equations used in most yield software, this provides an opportunity to make energy yield forecasts (and capacity and performance tests) more accurate. The realistic equation for radiative heat loss is available in our program, SunSolve Yield, where T_s is either loaded with the weather file or calculated from the Swinbank or Bliss models. When doing so, it is critical to reduce U_c so that it excludes radiative loss.

Readers are welcome to reach out to the SunSolve research team at support@sunsolve.com to learn more about thermal modelling, radiative losses, and the incorporation of radiative losses into yield forecasts. We hope this white paper inspires further research into the thermal modelling of PV systems.

8. References

[1] A. Driesse *et al.*, "Improving Common PV Module Temperature Models by Incorporating Radiative Losses to the Sky", *Sandia National Laboratories Report*, 2022.

[2] K.R. McIntosh *et al.*, "The influence of wind and module tilt on the operating temperature of single-axis trackers", *49th IEEE Photovoltaic Specialists Research Conference*, 2022. See also the related presentation: https://sunsolve.com/videos/influence_wind_module_tilt_operating_temperature_single_axis_trackers/

[3] M. Theristis, N. Riedel-Lyngskær, *et al.*, "Blind photovoltaic modeling intercomparison: A multidimensional data analysis and lessons learned", *Progress in Photovoltaics*, vol. 31, no. 11, pp. 1144–1157, 2023.

[4] P. Hamer *et al.*, "Improved thermal modelling of the 5B MAVERICK system: impact of sky temperature", *Asia-Pacific Solar Research Conf.*, 2023.

[5] M. Kim *et al.*, "Accurate modelling of module temperature for ground-mounted PV and its impact on degradation," submitted to *IEEE Journal of Photovolatics*, 2025.

[6] K.R. McIntosh *et al.*, "The Optimal Tilt Angle of Monofacial and Bifacial Modules on Single-Axis Trackers", *IEEE Journal of Photovoltaics*, vol. 12, pp. 397–405, 2021.

[7] Y. Tian *et al.*, "Understanding variations in downwelling longwave radiation using Brutsaert's equation", *Earth System Dynamics*, vol. 14, pp. 1363–1374, 2023.

[8] J. Muñoz Sabater, "ERA5-Land hourly data from 1950 to present.", *Copernicus Climate Change Service (C3S) Climate Data Store (CDS),* 2019, DOI: 10.24381/cds.e2161bac (Accessed Jun-2025)

[9] N. Riedel-Lyngskær, *et al.*, "Validation of Bifacial Photovoltaic Simulation Software against Monitoring Data from Large-Scale Single-Axis Trackers and Fixed Tilt Systems in Denmark", *Applied Sciences*, vol. 10, 8487, 2020.

[10] PVsyst, "Validations on old versions of PVsyst", *PVsyst* [Online]. Available: https://www.pvsyst.com/help-pvsyst7/validations_oldsystems.htm [Accessed: 25-Jul-2025]

[11] W.C. Swinbank, "Long wave radiation from clear skies", *Quarterly Journal of the Royal Meteorological Society*, vol. 89, pp. 339, 1963.

[12] R.W. Bliss, "Atmospheric radiation near the surface of the ground: a summary for engineers", *Solar Energy*, vol. 5, pp. 103–120, 1961.

[13] M.G. Lawrence, "The Relationship between Relative Humidity and the Dewpoint Temperature in Moist Air: A Simple Conversion and Applications", *Bulletin of the American Meteorological Society*, vol. 86, pp. 225–234, 2005.

[14] T.Q. Pean, "Nighttime radiative cooling potential of unglazed and PV/T solar collectors: parametric and experimental analyses", *Proc. of the 8th Mediterranean Congress of HVAC*, 2015.

[15] D. Faiman, "Assessing the outdoor operating temperature of photovoltaic modules", *Progress in Photovoltaics*, vol. 16, pp. 307–315, 2008.

9. Contributions

This white paper was written by the SunSolve Research Team at PV Lighthouse.

We thank the companies and institutes that generated the experimental data used in this study: FTC Solar, Sandia National Laboratories, 5B and the Technical University of Denmark (DTU). And we thank the following researchers for valuable discussion on thermal losses and measurements: Phill Hamer, Moonyong Kim, Zeinab Haydous, Shukla Poddar, Shaozhou Wang and Bram Hoex from UNSW; Rhett Evans and Mattias Juhl from 5B; Nicholas Riedel-Lyngskær from European Energy; Sergiu Spataru from DTU; Lance Brown, Ben Kahane and Saurabh Aneja from FTC Solar; Marios Theristis from Sandia National Laboratories; and Anton Driesse of PV Performance Labs.

We're also very grateful for the funding we receive from the Australian Renewable Energy Agency (ARENA) as part of ARENA's Advancing Renewables Program. The views expressed herein are not necessarily the views of the Australian Government, and the Australian Government does not accept responsibility for any information or advice contained herein.

Appendix A — Sky temperature models

Two useful models to estimate sky temperature T_s are those of Swinbank [11] and Bliss [12]. Swinbank's model depends only on the ambient temperature T_a,

$$T_s = 0.0552 \times {T_a}^{1.5}, \qquad (10)$$

whereas Bliss's model also incorporates the humidity via the dew-point temperature T_d,

$$T_s = T_a \times \left(0.8 + \frac{T_d - 273}{250}\right)^{1/4}, \qquad (11)$$

where the units of T are Kelvin in both equations.[13]

These models are compared to experimental data in Figure 15. The Swinbank model predicts the general trend of T_s vs T_a, but also it tends to overestimate T_s at dry sites like Albuquerque and Chajnantor, and understimate it humid sites like Singapore and Roskilde. The Bliss model is a better fit to the data at some sites (like Denver, Singapore and Roskilde) but not others.

See Kim *et al.* for more differences between satellite data and T_s models [5].

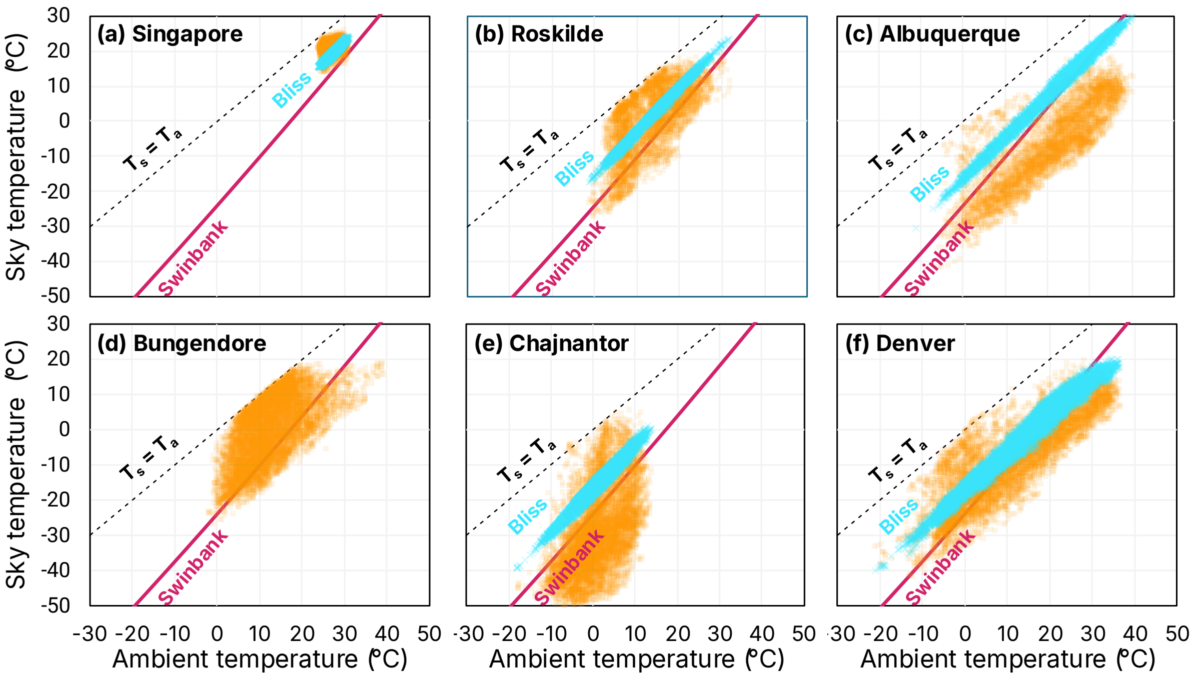

Figure 15: Sky vs ambient temperature measured in 2020 at six sites (see Section 5). Orange symbols plot experimental data. Swinbank and Bliss models also plotted.

[13] T_d is contained in many weather files but if it is not available, it can be estimated from T_a and the relative humidity (RH) by the Magnus formula: $T_d = 243.04 \times \gamma / (17.625 - \gamma)$, where $\gamma = \ln(RH/100) + 17.625 \times T_a / (243.04 + T_a)$ and RH is a percentage [13].

A comparison of the data to the Swinbank equation can provide a useful metric to assess other atmospheric effects. We demonstrate that with Figure 16, which plots ΔT_s against (a) humidity and (b) clearness index,[14] where ΔT_s is the difference between T_s calculated from ERA5 satellite data and T_s predicted by the Swinbank equation. The figure shows how the Swinbank equation underestimates T_s when the air is dry and clear and overestimates it when it is humid and cloudy. It also shows how these effects largely explain the difference between Albuquerque and Roskilde.

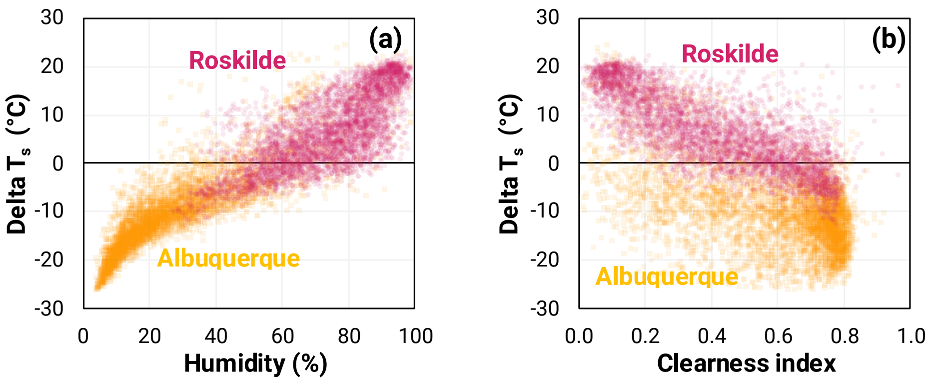

Figure 16: ΔTs vs **(a)** humidity and **(b)** clearness index at Albuquerque and Roskilde in 2024, where ΔT_s is the difference between T_s calculated from satellite data and the Swinbank model.

In summary, when satellite data is not available, the Swinbank model provides a first-order estimate of T_s, permitting a more accurate calculation of radiative losses than by using T_a. The Bliss model is only slightly superior to the Swinbank model.

[14] The fraction of direct light that passes through the atmosphere.

Appendix B — Thermal analysis of an SAT

In a study with FTC Solar, we examine three weeks of experimental data for a single-axis tracker (SAT) [2]. The data includes measurements of T_m, T_a and Φ, as well as wind speed and wind direction, in 5-minute intervals.

Standard approach to thermal modelling

We first predict T_m with the standard approach. That is, we feed the measured values of T_a and Φ into Eq (1), assume the conventional U-value of 29 $W{\cdot}m^{-2}{\cdot}K^{-1}$, and calculate T_m.[15]

Figure 17(a) compares that predicted T_m to the measured T_m for every data point. The discrepancy between the predicted and measured T_m is then quantified with two statistical metrics: the mean bias error (MBE), which is the average difference between all predicted and measured T_m; and the centred root-mean square error (CRMSE), which quantifies the scatter about the MBE. The CRMSE is equivalent to the standard deviation of the scatter.

As shown in the figure, the standard approach has an MBE of +2.9 °C and a CRMSE of 3.5 °C (daytime). To give these metrics context, they state that at any point during the daytime, the standard approach overestimates T_m by 3 ± 7 °C, where the uncertainty represents our 95% confidence interval. Not fabulous!

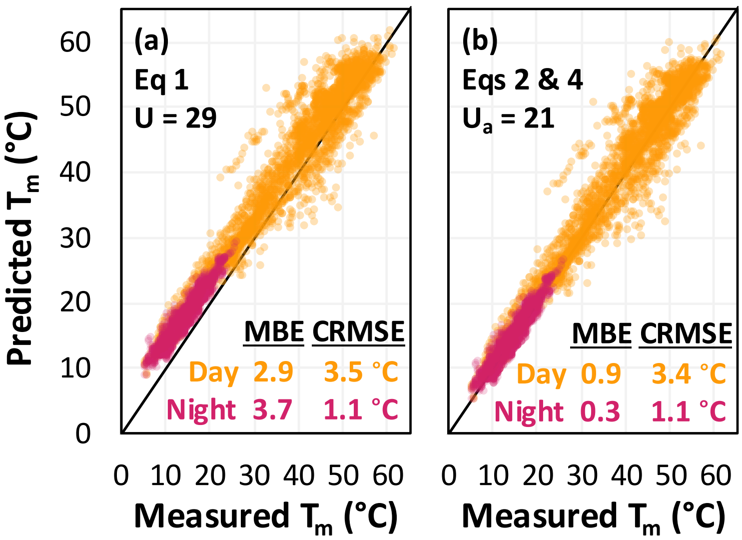

Figure 17: Predicted vs measured T_m for an SAT near Denver when using **(a)** Eq (1) with U = 29 $W{\cdot}m^{-2}{\cdot}K^{-1}$, **(b)** Eqs (2)and (4) with U_a = 21 $W{\cdot}m^{-2}{\cdot}K^{-1}$ and ε = 0.9.

[15] We make the standard assumption, α = 0.9, and calculate η as $\eta_{STC} \times (1 + \gamma \cdot (T_m - T_{STC})$ where η_{STC} = 18.3% and γ = −0.37%/K, as taken from datasheets for the experimental modules.

Nighttime data

It may sound odd for a PV researcher to be interested in nighttime data, but it is surprisingly useful. At night, when $\Phi = 0$ W/m^2, the standard approach to treating radiative heat loss necessarily predicts that $T_m = T_a$. That is, it assumes the module is in thermal equilibrium with the air. The data in Figure 17(a), however, shows that T_m is less than T_a by an average of 3.7 °C. This is clearer in Figure 18, which plots the measured T_m and T_a on a sunny day, illustrating how T_m falls below T_a at night.

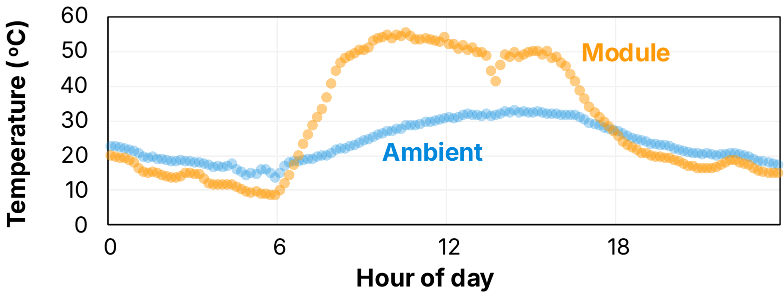

Figure 18: Measured T_m and T_a on a sunny day for the SAT near Denver.

What causes the nighttime discrepancy? While there must be some measurement error in T_m and T_a, this nighttime discrepancy is observed in all PV systems and is predominantly due to radiation to the sky [1–3, 14]. Since Φ = 0 W/m^2, we have $Q_a + Q_s = 0$ W/m^2, and combining Equations (2), (3) and (4) gives

$$U_a \cdot (T_m - T_a) + \sigma \cdot \epsilon \cdot \nu_s \cdot (T_m^4 - T_s^4) = 0, \qquad (12)$$

from which one can conclude that the module temperature must lie somewhere between the ambient and the sky temperature, $T_a > T_m > T_s$. Thus, heat flows from the air to the module and radiates from the module to the sky.

If we trust our inputs for T_s, T_a, η and v_s, we can therefore determine the nighttime U_a (the non-radiative heatloss coefficient), by finding the value for which the MBE of the nighttime data is zero. In this study, that gives U_a = 18.4 W·m^{-2}·K^{-1}. This value is not dissimilar to the U_a of 19.3 W·m^{-2}·K^{-1} that we calculated for our example system in Section 3. Thus, the nighttime data provides valuable information about the thermal behaviour of the system.

We expect, however, that the nighttime U_a should be lower than the daytime U_a because the days are windier than the nights (and the wind increases heat loss by forced convection). We therefore treat our calculation of the nighttime U_a as an interesting aside and return to using U_a = 20.9 W·m^{-2}·K^{-1} for our calculations, as estimated for the example system — which also happens to give a better fit to daytime data.

Initial assessment with the radiative equation

We next introduce the radiative equation into the analysis of the daytime data. That is, we set the non-radiative U-value to U_a = 20.9 W·m^{-2}·K^{-1} and use Eq (4) to calculate the radiative heat loss. These results are shown in Figure 17(b).

Figure 17(b) exhibits a much-improved MBE, which decrease from +2.9 °C to +0.9 °C, and a general slope that more closely matches the 1:1 line. Yet while this observation is heartwarming, we're not overexcited. Firstly, we are not sure that systematic error in the measurement of T_m, T_a and Φ did not introduced an error in the MBE of less than ±2 °C, which is required to be certain that the MBE improved. Secondly, the selected value of U_a was an estimate that might apply well here but not in other PV systems. And finally, and most importantly, we do not see a reduction in the CRMSE. That is, the inclusion of the more realistic equation for radiative heat loss into the basic equation has not increased our ability to predict the measured T_m.

Accounting for transient and wind effects

This investigation of radiative losses is much better served after accounting for two major sources of scatter: wind and transients. We account for transients using the calculated heat capacitance, mass and area of the module [2] (and no free variables), and we account for wind by expanding our definition of U_a. Following Faiman [15], we break U_a, which quantifies heat flow to the ambient, into two terms: U_v, which is the forced-convection term and U_c, which is everything else.

$$U_a = U_c + U_v \cdot w. \quad (13)$$

We also calibrate U_c and U_v to the SAT, such that they give the best fit to the experimental data, ensuring an MBE of zero and otherwise minimising the CRMSE.[16]

[16] $U_c + U_s$ = 25.3 W·m^{-2}·K^{-1} and U_v = 3.3 W·s·m^{-3}·K^{-1}.

Figure 19(a) plots the results when a simple account of radiative losses is applied Eq (3), and thus

$$\Phi \cdot (\alpha - \eta) = (U_c + U_v \cdot w) \cdot (T_m - T_a) + U_s \cdot (T_m - T_a), \qquad (14)$$

The figure shows that CRMSE is reduced from 3.5 to 2.8 °C, indicating that the accounting of transients and wind significantly reduces the scatter.

But notice the strange shape to the curve? At low irradiance, the error asymptotes at 3.7 °C (the nighttime error), but the data bends to ensure that the daytime MBE is zero. This is reminiscent of the error in Figure 1(a) resulting from excluding radiative losses.

Figure 19(b) plots the results of the same study, except that radiative losses are now treated more realistically with Eq (4), and hence[17]

$$\Phi \cdot (\alpha - \eta) = (U_c + U_v \cdot w) \cdot (T_m - T_a) + \sigma \cdot \epsilon \cdot v_s \cdot (T_m^4 - T_s^4). \qquad (15)$$

We now see (i) the non-linear trend is largely removed, and (ii) a large improvement in the daytime CRMSE, decreasing from 2.8 to 1.8 °C.

This is a very clear indication that accounting for radiative losses leads to a significant improvement in our ability to predict T_m. Our 95% confidence in predicting the measured T_m at any point during the day has decreased from ±5.6 °C to ±3.6 °C.

Importantly, we have not introduced any additional free variables.

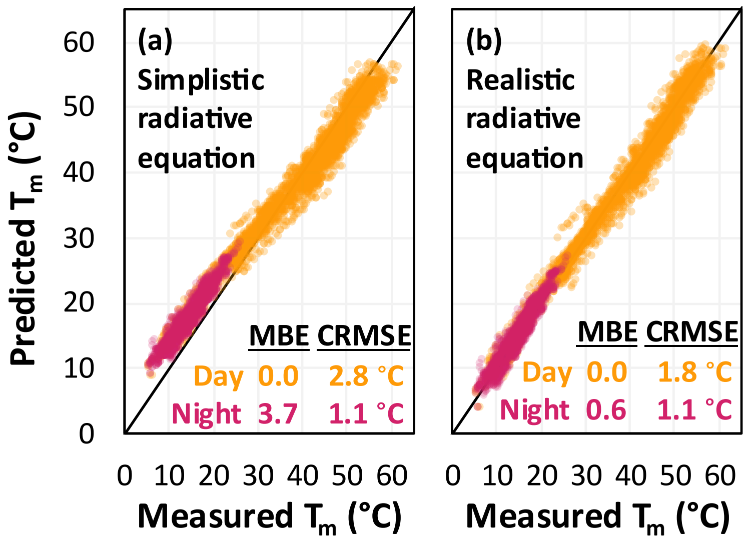

Figure 19: Predicted vs measured T_m for an SAT near Denver when accounting for radiation with the **(a)** simplistic and **(b)** realistic equation, using calibrated values for U_c, U_v and accounting for transient effects.

[17] U_c = 12.9 W·m^{-2}·K^{-1} and U_v = 3.2 W·s·m^{-3}·K^{-1}.

Refining the model further

We were curious to find out how much further we could improve the model. By extending convection loss to include tilt and wind direction, and accounting for the difference in temperature between the ambient and ground, we reduced the CRMSE a little further to 1.5 °C. These results are plotted in Figure 20. This is the model used to calculate the data shown in Figure 8 and on the title page of this white paper. It is described more in [2].

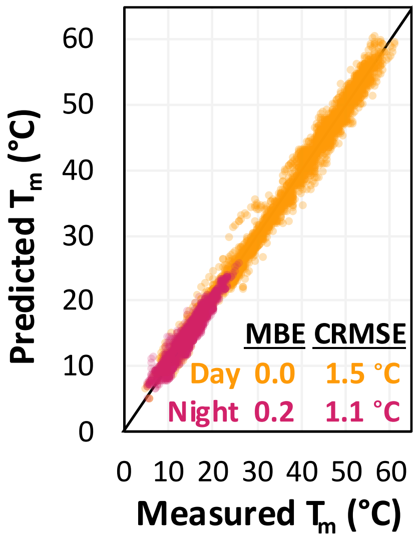

Figure 20: Predicted vs measured T_m for an SAT near Denver when using the realistic equation for radiative losses, calibrated values for U_c, U_v, and when accounting for transient effects, the effect of wind direction and tilt on convection, and ground temperature.

Appendix C — Advanced topics

Here are five interesting explanations on advanced topics:

Extracting T_s from downwelling longwave radiation

Downwelling longwave radiation, also known as 'downwards solar thermal radiation', is the longwave radiation emitted from the atmosphere towards the earth's surface. We represent it as Q_d in W/m^2 and convert it into an effective sky temperature T_s by assuming a unity sky emissivity and applying the Stefan-Boltzman Law, $Q_d = \sigma \cdot T_s^4$. The assumption for the sky emissivity is negated when calculating Q_s with Eq (4), which also assumes a unity sky emissivity. Driesse *et al.* neglect converting the downwelling to T_s altogether (Eq 15 in [1]) but we find it instructive to consider this 'effective T_s'. Kim *et al.* also uses downwelling and compares ERA and MERRA2 data alongside calculations from T_s models [5].

Radiative losses exceeding 100%

At sites with low irradiance, it is possible for the radiative heat loss to exceed the net heat loss from the module. How is that possible? This occurs when there is weak sunlight and the sky is much colder than the ambient air.

Like the nighttime case, when the irradiance is low, it is insufficient to heat the modules to an operating temperature T_m above T_a. Thus, the modules are warmed by the air and cooled by the sky, and the radiative loss can exceed the net heat loss from the module.

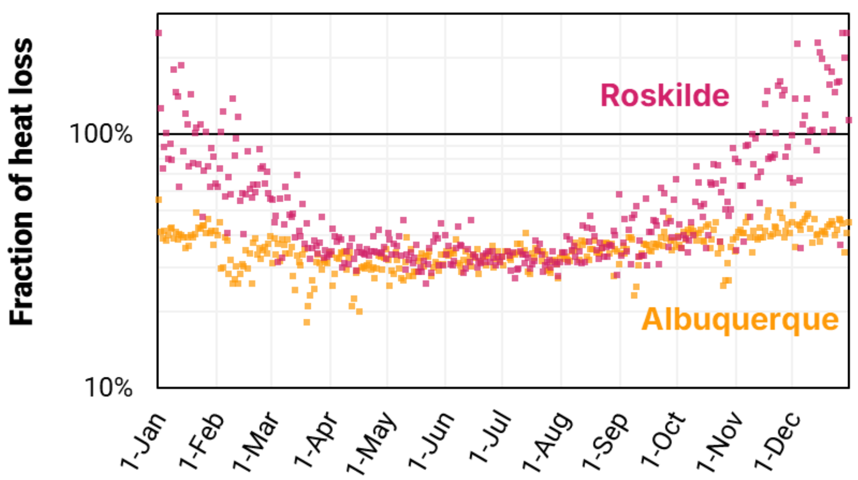

Figure 21: Fraction of heat lost to the sky vs day of year calculated for Roskilde and Albuquerque during daytime hours.

Why U_s increases with T_m

At first glance, one might expect U_s to increase with T_m. That is, one might expect that a higher module temperature would have a higher radiative heat loss coefficient. And that would indeed be true if one defined U_s relative to T_s. Consider that

$$Q_s = \sigma \cdot \epsilon \cdot v_s \cdot (T_m^4 - T_s^4), \quad (16)$$

can be rewritten

$$Q_s = \sigma \cdot \epsilon \cdot v_s \cdot (T_m^2 + T_s^2) \cdot (T_m + T_s) \cdot (T_m - T_s), \quad (17)$$

and thus, if one defines U_s with $Q_s = U_s \cdot (T_m - T_s)$, then

$$U_s = \sigma \cdot \epsilon \cdot v_s \cdot (T_m^2 + T_s^2) \cdot (\mathrm{T_m} + \mathrm{T_s}), \quad (18)$$

and U_s must increase with T_m and T_s and be independent of T_a.

But, in this work, we defined U_s with Eq (3), and thus,

$$U_s = \sigma \cdot \epsilon \cdot v_s \cdot \frac{(T_m^4 - T_s^4)}{(T_m - T_a)}, \quad (19)$$

Consequently, U_s always decreases with T_s, increases with T_a, and whether it increases or decreases with T_m depends on T_s and T_a.

This gives the curious feature that when one considers the total U-value defined by Eq (1), the contribution of radiative losses means that the U-value increases as T_m approaches T_a. In fact, it approaches infinity. This does not mean that the error in T_m approaches infinity (see Figure 1(a)).

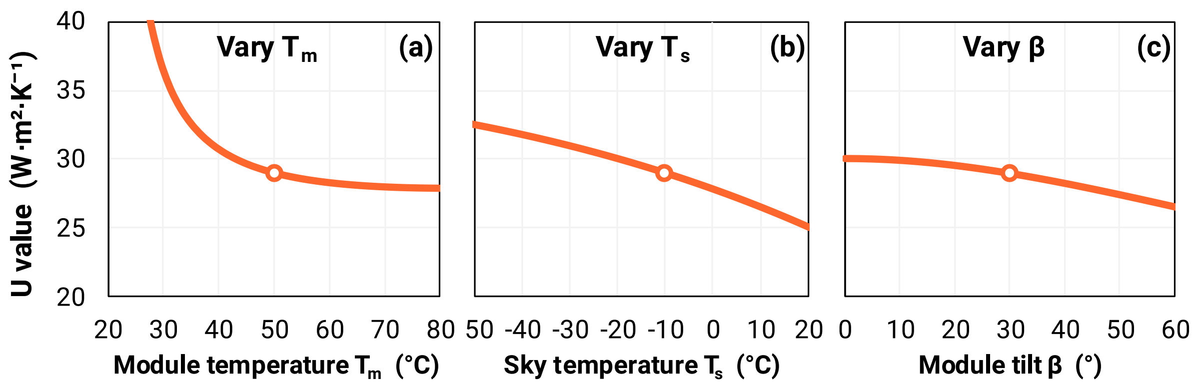

Figure 22: U_{tot} when calculating U_s with Eq (3) instead of Eq (4), assuming U_a = 19.7 W/m²/K, plotted for a range of **(a)** T_m, **(b)** T_s and **(c)** β for the conditions of Section 3.

Measurement offset

This paper focused on the error arising from a simplistic treatment of radiative loss to the sky. This error primarily arises because one computes the loss with T_a instead of T_s, which. in itself would not be a problem if ($T_a - T_s$) were roughly constant, but that is not always the case.

When we plot the predicted vs measured T_m, this error manifests as a sub-unity slope, as plotted below in Figure 23 (and evident in Figure 19). Such a slope is a signature of the error arising from a simplistic application of radiative loss.

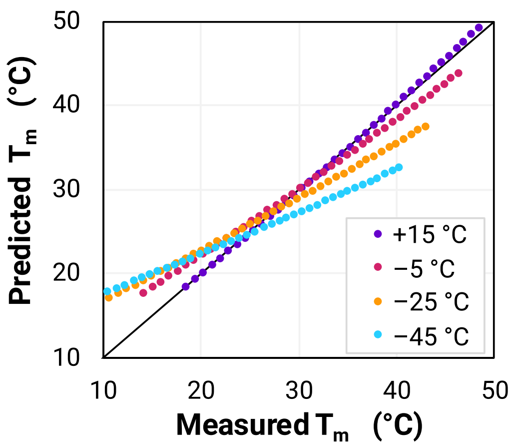

Figure 23: Pred vs meas T_m when calibrating U_s for a range of T_s when T_a = 15 °C.

Unfortunately, there is another source error that can have a similar sub-linear slope: a negative offset error in the measurement of T_m. Figure 24 demonstrates how such an offset introduces a non-unity slope when U is calibrated to give an MBE of zero. This can exacerbate or mitigate the slope from the radiative error.

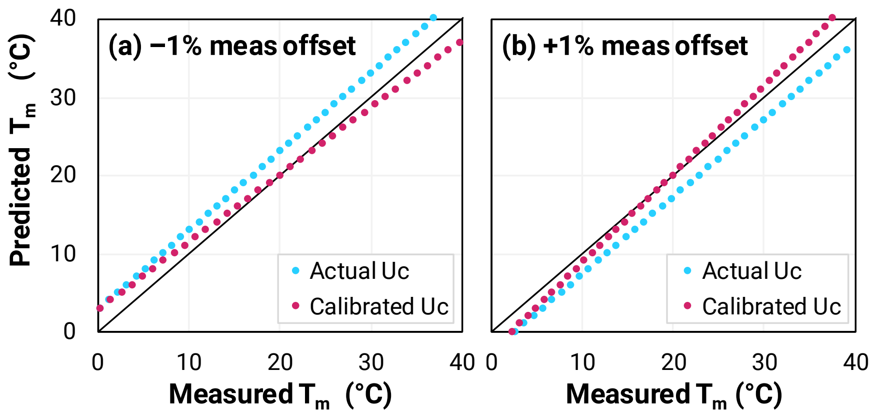

Figure 24: Pred vs meas T_m when measured T_m is offset by **(a)** –1% or **(b)** +1%. Two example datasets are plotted: one calculated for the actual U_c (unity slope and offset from 1:1 line) and another for the U_c value that gives MBE = 0% (non-unity slope).

A few complications

We have neglected many subtle complications, and mention a few here.

The temperature of a module is not the same everywhere: the rear surface, where T_m is usually measured, can be one or two °C smaller than the temperature of the cells, and the temperature across the panel can vary by a few °C.

We neglected to mention the rear-side irradiance and radiative losses, which were taken into account for the bifacial modules at Denver but not the monofacial modules at other sites.

The U_v value is normally calibrated to the wind speed at a height of 10 m. Measurements of wind speed at Bungendore, however, were made at a height of 1.6 m, which led to the calibrated U_v being higher than normal. Since the annual yield simulations were conducted using data for 10 m, we reduced the U_v by 25% as deduced from data for wind speed vs height.

Our annual yield simulations neglected clipping, which would reduce differences between modules and sites. The accuracy of T_m forecasts remains important, however, because it also affects degradation rates.

PVsyst applies the equation, $\Phi \cdot \alpha \cdot (1 - \eta)$, instead of $\Phi \cdot (\alpha - \eta)$ as derived by Faiman and used here.